INSTITUTE OF PHYSICS PUBLISHING PLASMA PHYSICS AND CONTROLLED FUSION

Plasma Phys. Control. Fusion **48** (2006) S51–S73 doi:10.1088/0741-3335/48/4/S05

Observation of turbulent-driven shear flow in a cylindrical laboratory plasma device

G R Tynan, C Holland, J H Yu, A James, D Nishijima, M Shimada and N Taheri

Department of Mechanical and Aerospace Engineering, University of California, San Diego, La Jolla CA 92093, USA

Received 31 August 2005, in final form 9 February 2006
Published 20 March 2006
Online at stacks.iop.org/PPCF/48/S51

Abstract

A turbulent-generated azimuthally symmetric radially sheared plasma fluid flow is observed in a cylindrical magnetized helicon plasma device with no external sources of momentum input. A turbulent momentum conservation analysis shows that this shear flow is sustained against dissipation by the turbulent Reynolds stress generated by collisional drift fluctuations in the device. In the wavenumber domain this process is manifested via a nonlinear transfer of energy from small scales to larger scales. Simulations of collisional drift turbulence in this device have also been carried out and clearly show the formation of a shear flow quantitatively similar to that observed experimentally. The results integrate experiment and first-principle simulations and validate the basic theoretical picture of drift-wave/shear flow interactions.

(Some figures in this article are in colour only in the electronic version)

1. Introduction

Inhomogeneous magnetized plasmas with a finite pressure gradient transverse to the magnetic field can develop 'electron drift waves' so-named because the waves propagate at the electron diamagnetic drift velocity V_{de}. These waves can subsequently grow to large amplitude, nonlinearly interact and develop into a turbulent spectrum. The theoretical properties of linear drift waves are well understood and were verified in a series of experiments [8–12, 15, 37, 64]. In the simplest manifestation of drift waves, a magnetized plasma with finite electron pressure and cold ions has a zeroth order azimuthal electron drift (needed to maintain equilibrium) which is unstable to azimuthal perturbations. As a result, variations in plasma density and electrostatic potential develop. In the presence of finite electron dissipation, rapid parallel electron motion cannot short-circuit the potential variations and, as a result of the ensuing fluctuating $\boldsymbol{E} \times \boldsymbol{B}$ guiding centre drift, the initial small amplitude perturbation can grow to finite amplitude. For a concise physical picture of these linear aspects of drift waves see e.g. [10].

Under some conditions, the drift wave linear dispersion relation permits three-wave interactions to develop and, as a result, the drift waves can develop a spectrum of subharmonic

and higher harmonic components [16, 79] by means of progressive 3-wave (and higher order) interactions which satisfy the frequency and wavenumber constraints $\omega_1 + \omega_2 = \omega_3$ and $\boldsymbol{k}_1 + \boldsymbol{k}_2 = \boldsymbol{k}_3$ [68]. With strong enough pressure gradients, a large enough system and enough parallel dissipation the coherent waves can become fully turbulent, resulting in the formation of broad frequency and wavenumber spectra and rapid turbulent transport of plasma across the confining magnetic field [47]. Drift instabilities are often classified according to the source of free energy and type of dissipation as discussed elsewhere [52]. We have documented the transition to drift turbulence in our device in a recent paper [5].

Most turbulent fluid flows are fully three-dimensional. In special cases, however, the turbulence can be reasonably described as occurring in two spatial dimensions. Examples of 2-d fluids include the thin atmospheres of terrestrial type planets, the atmospheres of rapidly rotating stars and gas giant planets, magnetized plasmas, rotating water tanks and stratified flows [6]. The distinction between two and three dimensions is important. In 3-d turbulence a finite strain field $\partial v_z/\partial z \neq 0$ causes vortex tube stretching (here z is aligned along the vortex axis), allowing both enstrophy production and energy transfer to smaller spatial scales where energy is dissipated by viscosity [65] in a process referred to as the turbulent energy cascade. In 2-d turbulence by definition the strain field vanishes, i.e. $\partial v_z/\partial z = 0$ and thus vortex tube stretching does not occur. As a result a dual cascade of energy and enstrophy occurs wherein the kinetic energy of the flow is transferred to the largest spatial scales in the system while the enstrophy is transferred to the smallest spatial scales [51]. When two like-signed vortices approach each other they merge into a larger scaled single vortex that does not suffer vortex stretching. As the merging process can then be repeated many times, progressively larger scaled structures can form. Eventually the kinetic energy of the flow condenses into long-lived, large-scale coherent structures [58, 75] and zonal flows [33, 35]—a picture that is fundamentally different from that of three-dimensional turbulence. The practical importance of these organized structures lies in their impact upon turbulent mixing and transport. For instance, self-generated zonal flows [33] and streamers [2, 21] represent two prominent examples of coherent structures relevant to magnetically confined plasmas which significantly impact turbulent transport.

As discussed earlier, in 2-d turbulent flows a condensation of the kinetic energy into a large-scale sheared zonal flow can occur. Such flows are thought to occur in magnetic fusion energy confinement devices; similar flows are also observed to exist in planetary and stellar atmospheres. These sheared flows are thought to be the result of such an inverse cascade, and thus are driven by nonlinear transfer of flow energy from the turbulence into the large-scaled shear flow via a three-wave coupling process satisfying the criteria $\boldsymbol{k}' + \boldsymbol{k}'' = \boldsymbol{k}_{\boldsymbol{ZF}}$ where $\boldsymbol{k}', \boldsymbol{k}''$ denote turbulent fluctuation wavenumbers and $\boldsymbol{k}_{\boldsymbol{ZF}}$ denotes the zonal flow wavenumber and in the idealized case $|\boldsymbol{k}'|, |\boldsymbol{k}''| \gg |\boldsymbol{k}_{\boldsymbol{ZF}}|$ [19] (we also note that higher order processes may be important as well [13] but here we focus upon the lowest order physics). The essential elements of this theoretical picture have been recently summarized in a review article [20].

Due to the importance of the problem a number of experimental studies of zonal flows have recently appeared in the literature. Probe measurements in the HT-6M tokamak device [82] show that the evolution of the turbulent Reynolds stress is consistent with the formation of the initial shear layer during a transition to improved Ohmic confinement in that device. Once the bifurcation event has been completed, strong radial ion pressure gradients can then act to sustain mean shear flow. An examination of probe data from the CCT, PBX-M and DIII-D devices showed that nonlinear coupling between low-frequency and higher frequency potential fluctuations exists and that this coupling evolves immediately prior to the L–H transition in the DIII-D tokamak [61, 77]. However these results provide no indication of the causality of the transition. In a series of papers Shats and co-workers [70–72,80,81] have shown that

low-frequency oscillating shear flows exist in the H-1 heliac device, that these shear flows modulate turbulent particle transport and are sustained by a transfer of energy from higher frequency turbulent fluctuations into low-frequency oscillations. These observations have many similarities to theoretical expectations for zonal flows in magnetic fusion confinement devices; however, the ions are unmagnetized in these experiments and thus the results may not be directly comparable with either existing theory [20] or to expectations for large magnetic confinement experiments. In the work on the CHS device, HIBP measurements have shown clear evidence of the existence of toroidally and poloidally symmetric time-varying shear flows in the core region of a toroidal device which are consistent with expectations for zonal flows [24]. There have also been observations of zonal flows in DIII-D using phase contrasting imaging [17] and applications of velocity inference techniques to beam emission spectroscopy measurements [42,57], and in the ASDEX machine via Doppler reflectometry [18]. A complete experimental demonstration of turbulent-generated shear flow requires several observations to be made in the same experimental apparatus. First, the existence of shear flow with correct symmetry properties (e.g. in a cylindrical plasma shear flow would be azimuthally symmetric) must be demonstrated. Second, shear flow must be maintained against damping mechanisms by the turbulent Reynolds stress or, equivalently [77], by the transfer of fluctuation energy from smaller turbulent scales into the larger shear flow scale via nonlinear mode–mode coupling processes. Third, the resulting shear flow must be of sufficient magnitude that it reduces or eliminates turbulent transport across the shear layer. Finally, this process should be consistent with a relevant theoretical description of the turbulence generation and shear flow maintenance mechanisms.

In this paper we provide experimental evidence that all these criteria are met during the development of a shear layer in a simple plasma system. In particular we provide evidence that a transfer of energy from collisional drift turbulence fluctuations with intermediate wavenumbers ($0.2 < k_\theta \rho_S < 1$) into linearly stable small wavenumbers ($k_\theta \rho_S < 0.1$–0.2) occurs. We show that these small wavenumber fluctuations correspond to an azimuthally symmetric radially sheared $E \times B$ plasma flow and we provide measurements of the turbulent particle flux and turbulent Reynolds stress. Using these results in the turbulent momentum conservation equation, we show that the observed shear flow is maintained against the estimated damping by these turbulent fluxes. Finally, we carry out a fluid-based two-field turbulence simulation of the experiment in the real geometry of the experiment. The simulation results are in quantitative agreement with the experimentally observed shear flow and they show how shear layer formation naturally emerges from the merging of tilted anisotropic vortices that emerge from the linear eigenmodes during the nonlinear saturation of the turbulence. This phenomena is a time–space domain representation of the inverse energy transfer process which is expected to occur in wavenumber space and is completely consistent with our experimental observations.

2. Experimental apparatus

The CSDX plasma source used an azimuthally symmetric half-wavelength helicon antenna operating at 13.56 MHz with 1500 W of forward power (less than 20 W are reflected and measurements indicate a high (80–90%) coupling efficiency with the plasma) with an argon gas pressure of 3.0 mTorr. The device exhibits the usual signs of helicon mode operation (i.e. equilibrium plasma density n_0 proportional to magnetic field B, transition to high density operation ($n_0 >$ few $\times 10^{12}$ cm^{-3}) for high enough B field (>400 G) and high enough source power (∼1 kW) and high enough fill pressure (>1 mTorr argon).

The present plasma source radius is approximately 4.5 cm, and is connected to a downstream chamber approximately 3 m long and having a 10 cm radius which is immersed

within a solenoidal magnetic field of up to 1 kG. The field lines located within $r < 4.5$ cm terminate on insulating surfaces in the plasma source, while source region field lines with $r > 4.5$ cm terminate on an insulating plate that covers the flange that mates the plasma source to the downstream chamber. On the other end of the device the field lines terminate on a series of ten concentric biasable end rings located 160 cm downstream of the plasma source exit which can be used to impose a radial electric field and azimuthal plasma flow. In the region beyond the end ring assembly, the vacuum chamber walls are covered with a thin sheet of teflon to prevent the diverging field lines, which pass through the gaps located between the end rings, from contacting a conducting surface. In all the experiments reported here, the end rings are left electrically isolated, prohibiting radial plasma currents (and thus azimuthally directed torques) from existing in the plasma. All the data shown in this paper are obtained at a distance of 75 cm downstream from the exit plane of the plasma source, approximately half the distance from the source exit to the end ring assembly. Detailed spatio–temporal measurements of equilibrium and fluctuating density, potential and electron temperature are made with various moveable probe arrays. Line averaged ion and neutral gas temperatures are measured using an optical fibre that transmits a central plasma chord view to a high-resolution spectrometer. A detailed description of the plasma source and fluctuation characteristics, mode identification and transition to turbulence can be found in the literature [5, 26, 76].

3. Experimental results

Data showing typical time-averaged plasma density and electron temperature profiles are shown in figures 1(*a*) and (*b*) below. Measurements in CSDX show the onset of low frequency (few kiloHertz) density and floating potential fluctuations ($\omega \ll \Omega_{C_i}$) with peak amplitude near the maximum in grad-n_0 for magnetic fields above a critical value (400–500 G) such that $\rho_S/L_n \sim 1$. The rms-floating potential fluctuation amplitude is shown in figure 1(*c*). Frequency-resolved radial profiles of the floating potential fluctuations are shown in figure 1(*d*). The measurements near onset conditions show these fluctuations are low order ($m = 1$–6) azimuthal drift wave eigenmodes propagating in the electron diamagnetic direction. As the magnetic field is increased a controlled transition to drift turbulence then occurs [5]. Thus we conclude that we can produce coherent drift wave oscillations and a controlled transition to drift turbulence in this device by using the external magnetic field as a control parameter.

During the evolution to turbulence we observe a gradual increase in the importance of three-wave coupling as evidenced by the large increase in the bicoherence, which measures the degree of phase coherence between different frequencies [5]. Density and potential fluctuations are highly correlated (power weighted average cross-coherence is ∼0.7 or higher) and have a small phase shift (power-weighted average phase delay is ∼0.2 rad or less)—results that are all consistent with the existence of collisional drift fluctuations in this plasma. When strong enough (i.e. at high enough magnetic field) these wave–wave interactions produce broad spectra as shown in figure 2, which shows the local wavenumber spectrum obtained at $r = 3$ cm (i.e. in the strong density gradient region) using the two-point technique [1]. As the magnetic field is raised from 500 to 1000 G a state of turbulence is approached and we observe the 'filling in' of the $k\rho_s < 1$ portion of the energy spectrum $E_k = (n_k^2/n_0^2) + k_\theta^2(e\phi_k/k_B T_e)^2$ (figure 3), which is obtained by integrating the two-point density and potential fluctuation spectra n_k^2/n_0^2 and $(e\phi_k/k_B T_e)^2$ over all frequencies. A detailed discussion of this transition to turbulence is given elsewhere [5], and we also note that these fluctuations appear to be quite similar to those reported earlier by Light *et al* [54] in another helicon plasma device similar to that used in our work. We have also shown elsewhere [78] that the low k region ($k_\theta \rho_S < 0.1$–0.2) is

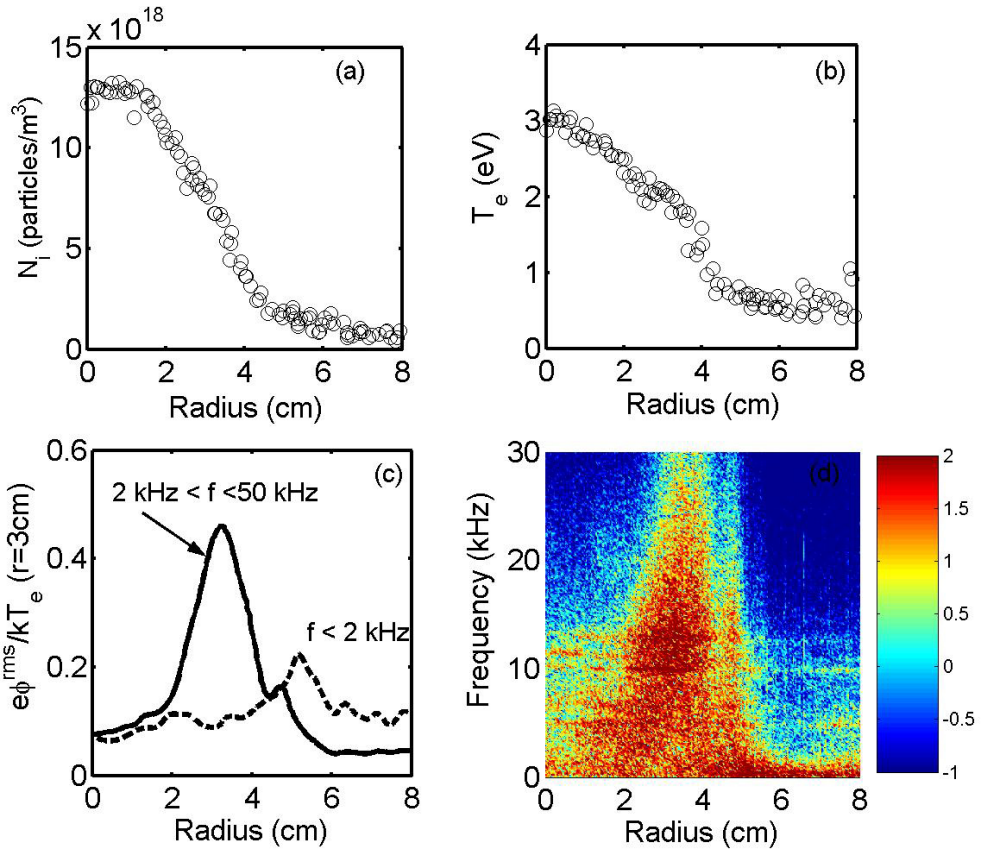

Figure 1. (*a*) Time-averaged plasma density profile. (*b*) Time-averaged electron temperature profile. (*c*) Floating potential RMS-fluctuation profiles for low-frequency $m \sim 0$ and higher frequency finite m fluctuations. (*d*) Radially resolved floating potential frequency spectrum.

linearly stable (figure 4). Thus the appearance of finite energy in this portion of the spectrum as the turbulent state is approached implies that these low k fluctuations are driven via some nonlinear process. We thus conclude that the evolution of the drift fluctuations in the CSDX apparatus is consistent with the existence of an inverse energy transfer from drift turbulence that can be grown from a known free energy source and dissipation mechanism in a controlled manner.

The radial distribution of the local wavenumber spectra is obtained by integrating the two-point spectra obtained at $r = 3, 4$, and 5 cm over all frequencies. The results of this procedure are shown in figure 5. The data clearly show that the mean wavenumber k_θ of the fluctuations falls from finite values $k_\theta \rho_S \approx 1$–2 at $r = 3$ cm (corresponding to an azimuthal mode number $m = 3$–6), where the largest plasma pressure gradient is located, to $k_\theta \rho_S \approx 0$ at $r \geqslant 4$ cm (corresponding to $m \sim 0$). These large azimuthal wavelength fluctuations correspond to the very low frequency (<2 kHz) potential fluctuations that are seen in figure 1(*d*) in the region $3 < r < 6$ cm, and they correspond to the linearly stable portion of the wavenumber spectrum shown above in figure 4. These observations demonstrate that an $m = 0$ low frequency oscillation in the plasma potential exists in the region between 4 and 6 cm. The radially resolved data show that these oscillations have a definite radial structure. These fluctuations are linearly stable and thus by implication must be maintained by some nonlinear process.

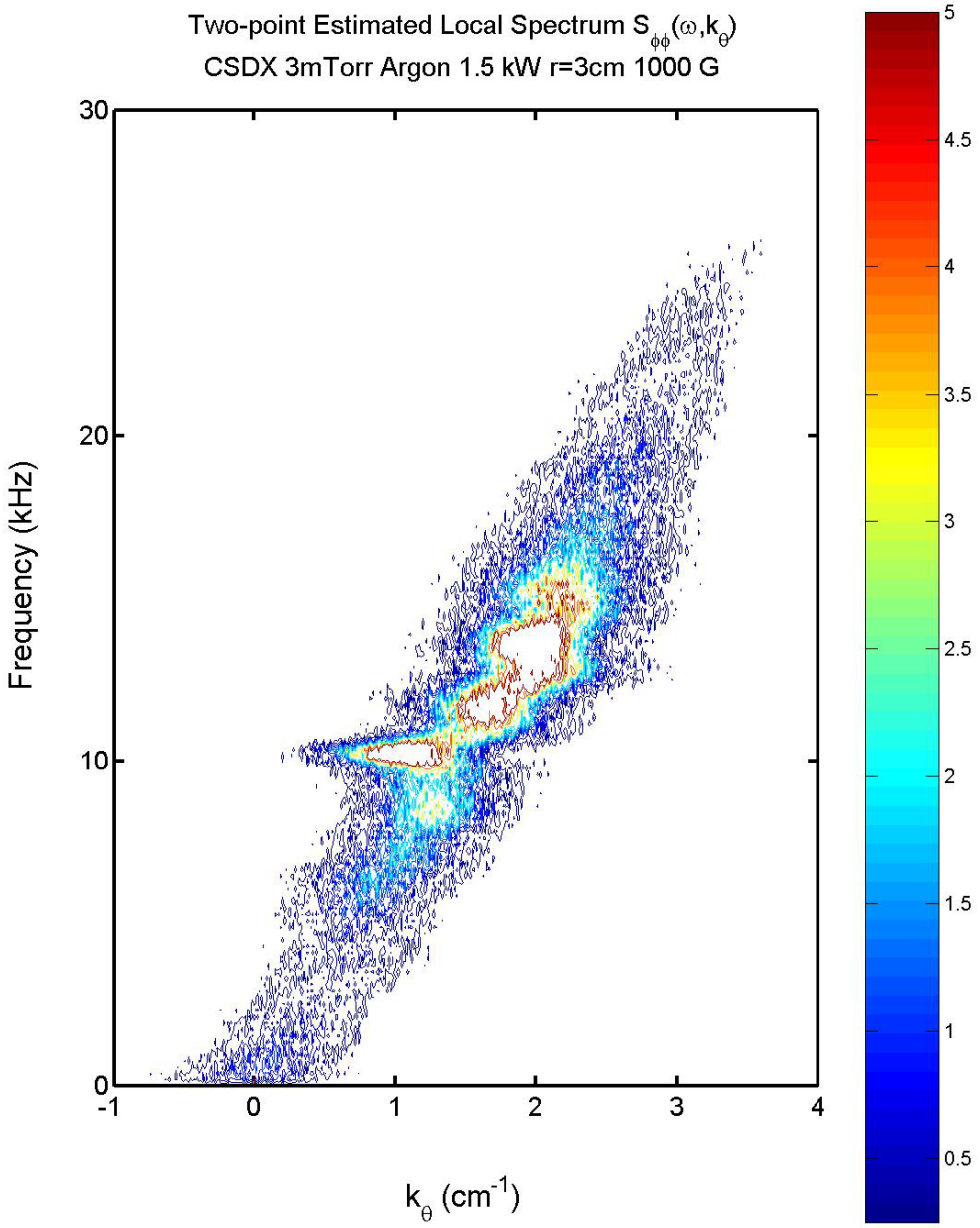

Figure 2. Frequency and wavenumber resolved two-point spectrum obtained from floating potential fluctuations at $r = 3$ cm.

We have used two different techniques to determine the existence of a velocity shear layer. First, we measured the radial profile of the mean azimuthal fluctuation velocity using time-delay estimate (TDE) techniques [38]. In this technique the density (or potential) fluctuations at two azimuthal positions separated by 0.5 cm are sampled with high time resolution (10^6 samples s^{-1}) and then the small time incurred by the propagation of the fluctuations between the two probes is measured. The velocity is then taken as the spatial

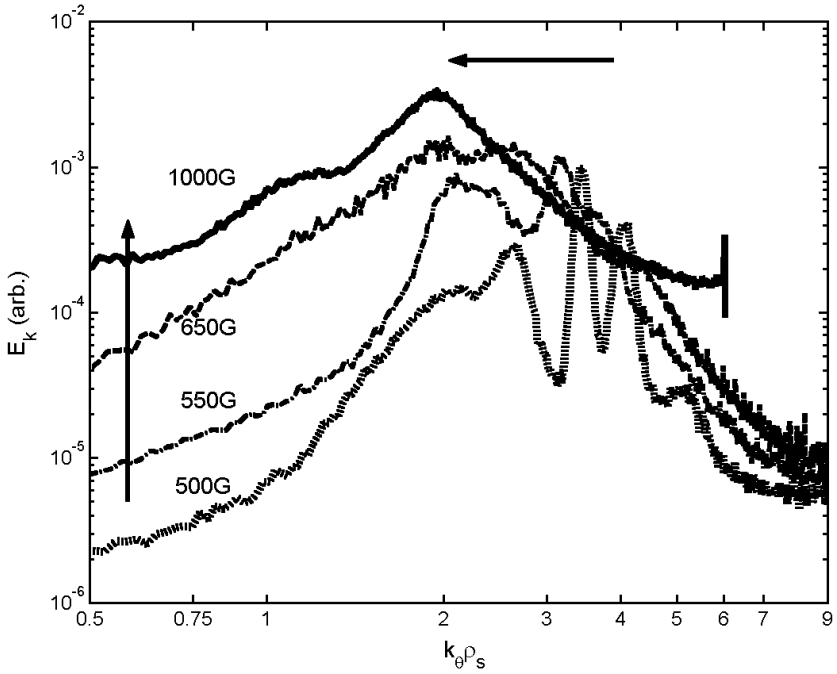

Figure 3. Evolution of the total energy spectrum as the magnetic field is raised from the threshold for onset of drift waves (400 G) to 1000 G where turbulent spectra are observed. Data obtained at $r = 3$ cm.

separation divided by this measured time delay (determined by where the cross-correlation function of the two channels peaks). The results are shown as the open diamond-shaped symbols in figure 6. These data show that the azimuthal velocity has a strong radial variation and is peaked at $r = 3.5$–4.5 cm, indicating the presence of a plasma shear layer at this location. Similar measurements made using a series of fast (100 kHz) framed images of plasma light emission show that this azimuthal fluctuation propagation is azimuthally symmetric.

Second, in order to demonstrate that the plasma fluid is rotating (as opposed to simply a propagation of fluctuations without any underlying fluid $E \times B$ flow), we have also used a multi-sided Mach probe to infer the parallel and perpendicular Mach number profiles using recently published techniques [73]. The ion fluid velocity is measured with a Mach probe that is inserted along the radius of the plasma and rotated about the probe shaft axis on a shot-to-shot basis. The probe is scanned across the plasma radius and the ratio $R_{\rm M} = I_{\rm sat}({\rm up})/{\rm I}_{\rm sat}({\rm down})$ of collected ion saturation currents obtained from 180°-opposed probes is measured as a function of position. The procedure is then repeated for various angles θ thereby yielding a measurement of $R_{\rm M}(\theta)$ as a function of radius. Here $I_{\rm sat}$ (up) and $I_{\rm sat}$ (down) denote the probe tips that are located upstream (closer to the plasma source) and downstream (farther from the plasma source), respectively. We then fit $R_{\rm M}(\theta)$ to a recent theory prediction [73] of the form $R = \exp[K(\sin\Delta\alpha/\Delta\alpha)(M_{\rm par}\cos\theta + M_{\rm perp}\sin\theta)]$ using the parallel and perpendicular Mach numbers $M_{\rm par}$ and $M_{\rm perp}$ as the fitting parameters. Here $\Delta\alpha$ denotes the acceptance angle of an individual ion-collecting probe tip ($\Delta\alpha \sim 50°$ in our probe). An example of such a fit to the data obtained at $r = 3.5$ cm is shown in figure 7, yielding $M_{\rm par} = 0.29$ and $M_{\rm perp} = 0.16$. For our data presented here, we use Hutchinson's model of ion collection

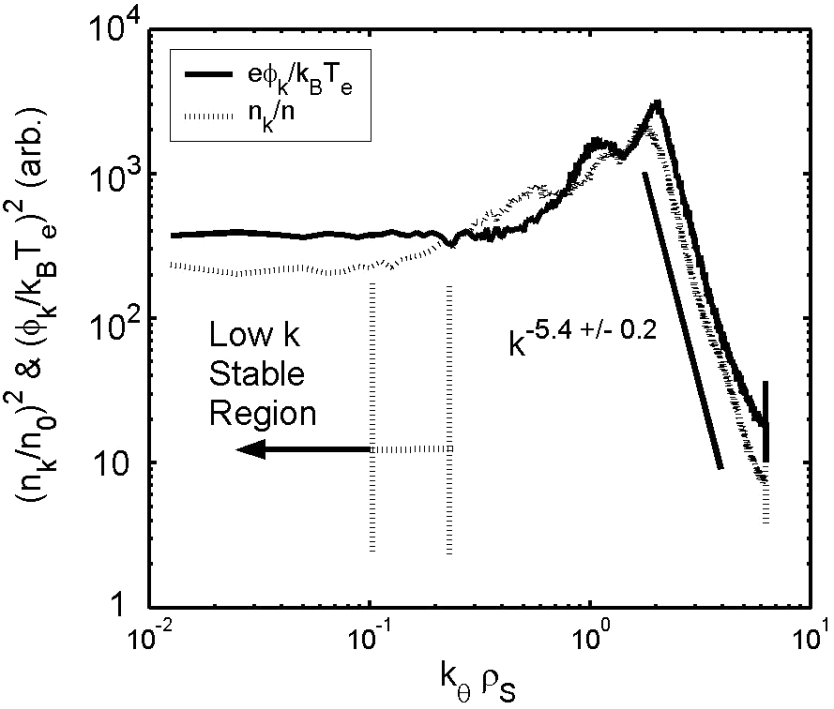

Figure 4. Ion saturation current and floating potential azimuthal wavenumber spectra at 1000 G. Data taken at $r = 3$ cm.

giving the constant $K = 1.34$ [41]. These measurements are then repeated at a variety of radial positions, and the electron temperature is then used to translate the Mach number into a plasma fluid velocity. The azimuthal velocity inferred using this technique is shown where the open square data points in figure 6 and is found to agree with the TDE velocity at radii where the pressure gradient is small, while in regions where the pressure gradient is significant, the TDE velocity is larger than the Mach probe velocity, suggesting that the TDE technique is measuring an $E \times B$ Doppler-shifted diamagnetic drift. A detailed paper on the relationship between TDE velocity measurements and plasma fluid flow is in preparation and will be presented elsewhere.

The experimental results thus show that a velocity shear layer exists in this plasma (which has no external sources of momentum such as a cross-field current flowing between a cathode and an anode) and that the velocity shear layer is azimuthally symmetric. This shear layer is also strikingly similar to the one reported recently in a similar helicon plasma device, measured unambiguously with laser induced flourescence [29]. The location of this shear layer also coincides with the location of the $m = 0$ structure that was inferred from the results shown earlier in figure 5 and, as we have shown elsewhere [78], the shearing rate is sufficiently strong to affect the underlying turbulence in the vicinity of the shear layer.

As we show below, this shear is damped by ion–neutral drag as well as by ion–ion collisional viscosity. Some mechanism must exist in order to maintain the shear flow against this damping. As discussed earlier, there are no externally driven currents in this experimental apparatus. Thus attention naturally turns to the role that turbulent momentum transport plays in possibly maintaining the shear flow.

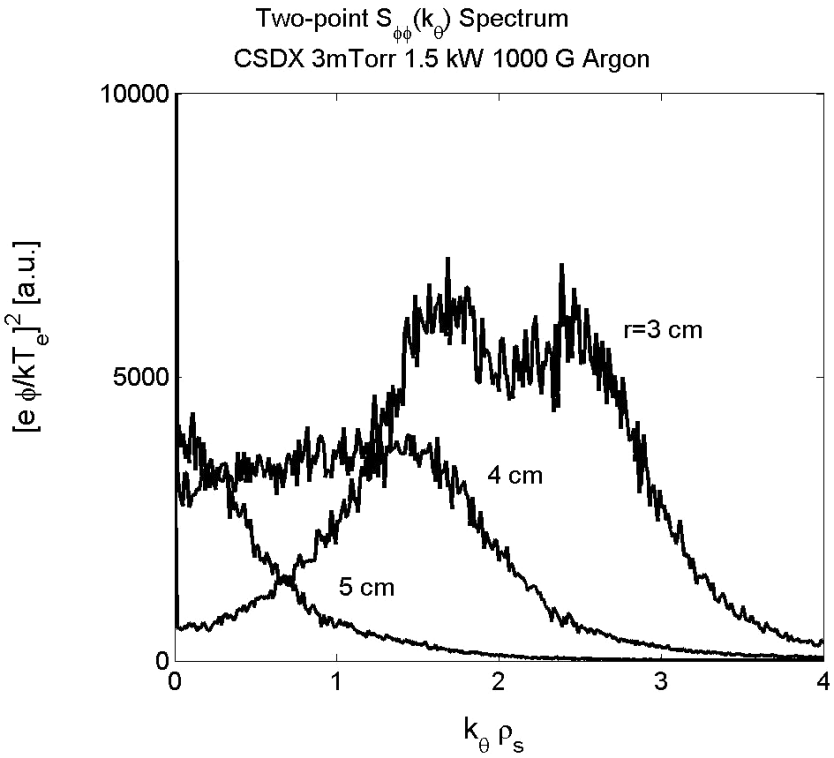

Figure 5. Azimuthal wavenumber spectra of floating potential fluctuations at $r = 3$, 4 and 5 cm.

4. The turbulent momentum conservation equation

In the presence of a finite ion–neutral momentum dissipation rate $\nu_{\text{i–n}}$ and finite ion–ion collisional viscosity μ_{ii}, the relationship between the radial profile of the mean azimuthal plasma fluid velocity and the turbulent Reynolds stress is given by the time-averaged azimuthal component of the ion momentum equation:

$$\frac{1}{r^2}\frac{\partial}{\partial r}(r^2\langle\tilde{V}_{\text{r}}\tilde{V}_\theta\rangle) = -\upsilon_{\text{i–}n}\langle V_\theta\rangle + \mu_{\text{ii}}\frac{\partial^2\langle V_\theta\rangle}{\partial r^2} + \frac{1}{r}\frac{\partial\langle V_\theta\rangle}{\partial r} - \frac{\langle V_\theta\rangle}{r^2}, \tag{1}$$

where the brackets denote a time average and tildes fluctuating quantities, such that $\langle V_\theta\rangle$ is the time-averaged azimuthal ion fluid velocity, $\nu_{\text{i–}n}$ is the ion–neutral collision rate and μ_{ii} is the ion viscosity. A detailed derivation of this equation is given in the appendix. Using a four-tip Langmuir probe assembly (which allows us to measure density and electric field fluctuations simultaneously) we have measured the electrostatic turbulent Reynolds stress $\langle R\rangle = \langle\tilde{E}_{\text{r}}\tilde{E}_\theta\rangle/B_0^2$ (equal to $-\langle\tilde{V}_{\text{r}}\tilde{V}_\theta\rangle$ under the assumption that the convecting velocity fluctuations are purely electrostatic) and the turbulent particle flux $\langle\Gamma_{\text{r}}\rangle = \langle\tilde{n}\tilde{v}_{\text{r}}\rangle = \langle\tilde{n}\tilde{E}_\theta\rangle/B_0$, where $\tilde{E}_{\text{r}} = \Delta V_{\text{f}}/\Delta x_{\text{r}}$ is the fluctuating radial electric field taken as the difference between the floating potentials measured with two tips separated radially by a distance $\Delta x_{\text{r}} = 0.3$ cm; the fluctuating azimuthal electric field $\tilde{E}_\theta = \Delta V_{\text{f}}/\Delta x_\theta$ is measured similarly. Because we are interested in the origins of azimuthally symmetric shear flows, the relevant time average is taken to be the time required for a complete azimuthal rotation within the shear layer (estimated here to be ~ 0.4 ms for the conditions of our experiment). This time averaging

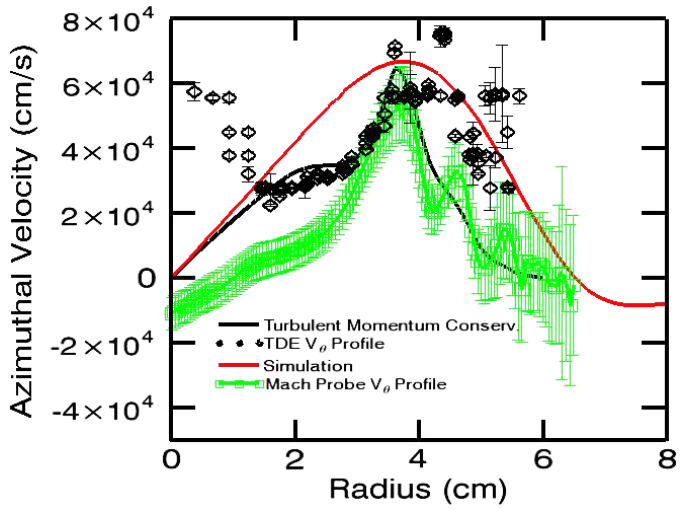

Figure 6. Radial profile of the azimuthal velocity profile measured with time-delay estimation technique (◊); Mach probe (□); Velocity profile inferred from turbulent momentum balance analysis (——) and velocity profile predicted by collisional drift turbulence numerical simulation (——). Mach probe experimental errors show 95% confidence interval from least squares fit. TDE error bars determined from shot-to-shot scatter of the data.

process therefore includes only fluctuating components with $m > 0$ in the computation of the Reynolds stress. Figures 8(*a*) and (*b*) show the measured $\langle \Gamma_r \rangle$ and $\langle R \rangle$ profiles. All the time-averaged data presented in this letter was obtained by averaging approximately 32 000 points of data sampled at 1 MHz taken with the probe assembly held fixed at 193 different spatial locations. Because CSDX can operate in a steady-state fashion for much longer time-scales, all our estimates of time-averaged quantities are extremely well converged, with the statistical error bars generally being within the thickness of the plotted mean value curves. The particle flux peaks in the region of the plasma pressure gradient, while the Reynolds stress profile peaks slightly farther out radially. Note in particular that there appears to be a close link between the fall off of radial particle flux and the onset of momentum transport via the Reynolds stress, suggesting a potentially important link between these two fluxes. The detailed spatial structure of the two fluxes is caused in part by significant changes in the zero-time delay cross-correlation coefficient computed between the density and azimuthal electric field fluctuations (figure 8(*c*)) or between the fluctuating azimuthal and radial electric fields (figure 8(*d*)). Both cross-correlation coefficients pass through zero near $r = 3.5$ cm, thereby causing the associated fluxes to also vanish at this location. This behaviour simply indicates that on average there is no radially directed turbulent mixing of either density or azimuthal momentum fluctuations across the $r = 3.5$ cm surface which, referring to figure 6, is seen to correspond to the location of the beginning of the velocity shear layer. Thus there is indeed a 'transport barrier' at this location both for particles as well as azimuthal momentum. Here the term transport barrier refers to an elimination of the turbulent particle and momentum flux, as opposed to a localized increase in the mean gradients, as is often the implied meaning in experiments on fusion confinement devices. The small inwardly directed particle flux in the region beyond the shear layer would be consistent with the existence of a small ionization source located in this plasma region which supplies particles that are advected inwards towards the shear layer.

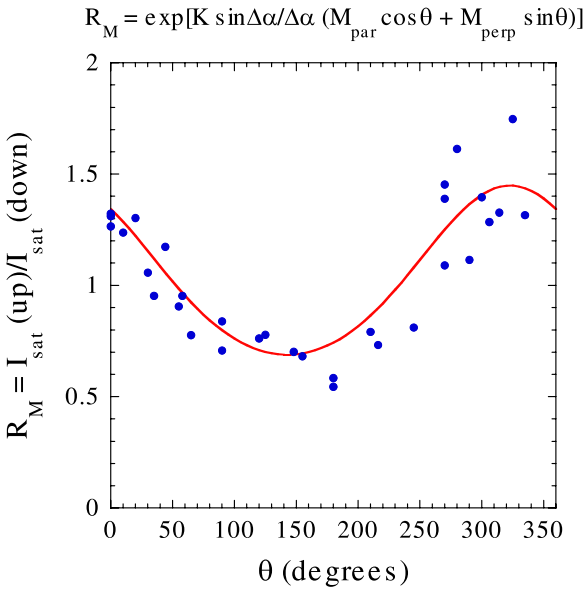

Figure 7. Ratio of upstream to downstream ion saturation current density versus angle of probe tips with respect to the magnetic field. Data points show measured values and the solid line shows a best fit to the theoretical expression shown in the figure.

Taking the measured Reynolds stress shown in figure 8, we can then solve equation (1) for $\langle V_\theta \rangle$ if the viscosity and neutral damping rates are known. Using reasonable boundary conditions (i.e. $\langle V_\theta \rangle \to 0$ at $r = 0$) the solution can be found numerically by integrating this equation from $r = 0$ outwards. The ion–neutral momentum dissipation term is proportional to the neutral gas density and ion–neutral momentum exchange cross-section. Since the neutral gas presumably follows an ideal gas law, a measurement of the neutral gas temperature in the centre of the plasma combined with a neutral gas pressure measurement at the wall can be used to estimate the central neutral density. If the neutrals are close to room temperature at the wall (which is a reasonable assumption) then the neutral gas density there can be easily computed from the measured pressure. The ion collisional viscosity scales as $N_\mathrm{i}/T_\mathrm{i}^{1/2}$, where N_i denotes the ion density and T_i denotes the ion temperature. Thus both the ion–neutral and ion–ion collisional dissipation processes require measurement of neutral argon and singly ionized argon in the central region of the plasma column.

These two temperatures were measured from a Doppler broadening of the 488 nm (Ar-II) and 750 nm (Ar-I) emission lines using a high resolution spectrometer. Plasma light was collected by an optical fibre connected to a collimating lens which collected light from a 0.5 cm diameter chord that passed through the plasma centre 0.5 m downstream from the exit of the plasma source. The fibre was connected to an ELIAS 10 m focal length echelle spectrometer (manufactured by LTB Gmbh, Berlin, Germany), which consists of a 30 cm-wide echelle grating configured in a Littrow configuration [30, 31]. The echelle grating with a focal length of 10 m gives extremely high spectral resolution ($\lambda_0/\Delta\lambda = 2.5 \times 10^5$, where $\Delta\lambda$ is the linewidth at the wavelength λ_0) giving a Gaussian instrumental FWHM of 1.7 pm for the lines of interest here. However, this configuration gives overlapping or aliased spectra due to higher/lower order light reflections within the optical train. In order to avoid this problem, a suitable optical band pass filter was placed between the optical fibre and the instrument. For the conditions of our experiment, collisional broadening and line splitting are negligible. Light was then collected

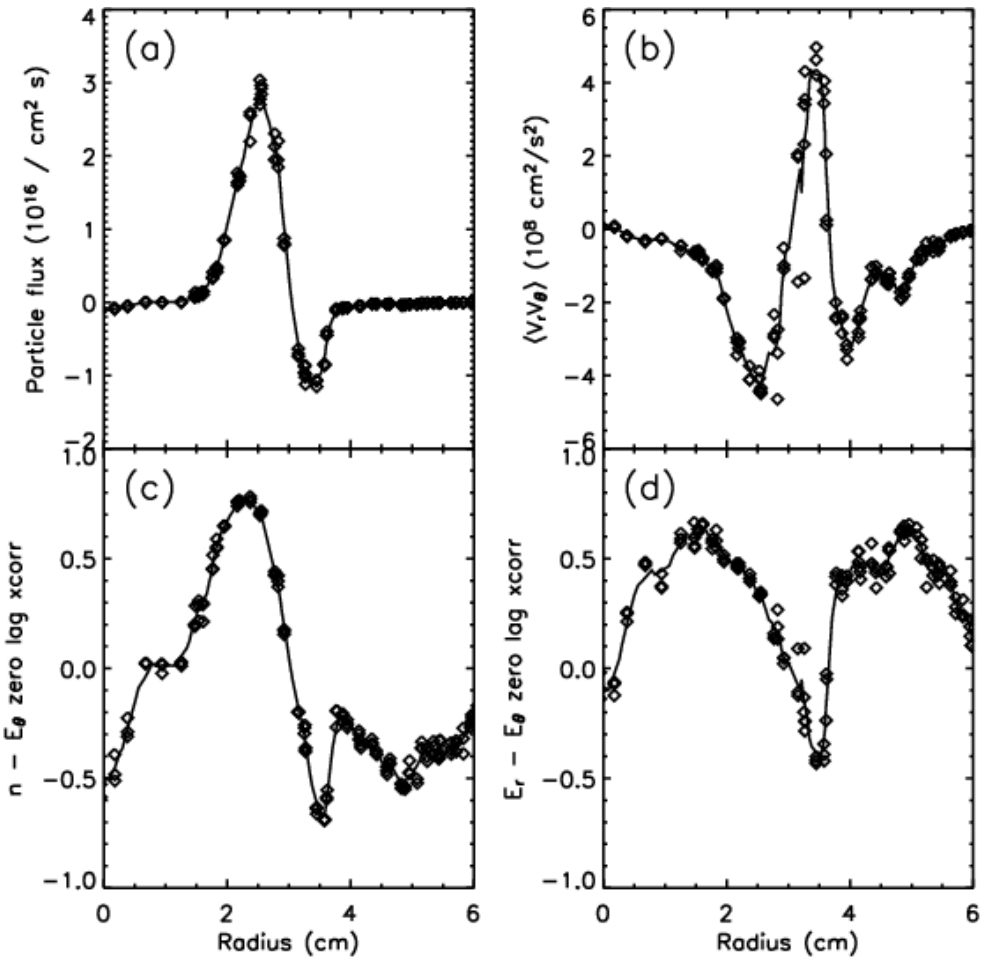

Figure 8. Radial profiles of the measured (*a*) turbulent particle flux, (*b*) turbulent Reynolds stress, (*c*) zero time-delay cross-correlation coefficent computed between density and azimuthal electric field fluctuations and (*d*) zero time-delay cross-correlation coefficient computed between radial and azimuthal electric field fluctuations. The random uncertainty in the particle flux and Reynolds stress is similar in size to the symbols used to display the data.

from the strongest emission lines of Ar-I and Ar-II (750 nm and 488 nm, respectively) for a 30 s integration period; the result was deconvolved from the instrument function, and the resulting Gaussian lineshape was then used in a least squares fitting procedure to yield line-averaged neutral and ion temperatures of 0.5 eV and 0.7 eV, respectively, for the neutral and singly ionized argon. Detailed discussions of these measurements are being prepared for publication elsewhere.

Using these temperatures, we estimate an ion viscosity $\mu_{\rm ii} = 3/10\rho_i^2 \nu_{\rm ii} \approx 4 \times 10^4\ {\rm cm}^2\ {\rm s}^{-1}$ in the central region of the plasma column. For a spatially uniform 3 mTorr fill pressure at $T_{\rm gas} = 0.5$ eV we estimate the average neutral gas density within the plasma as $n_{\rm gas} = 4 \times 10^{12}\ {\rm cm}^{-3}$. Note that this value corresponds to strong central gas depletion due to gas heating. Using published data for the total ion–neutral scattering cross-section for argon [55] we then estimate the ion–neutral momentum damping rate $\nu_{\rm i0} = n_{\rm gas} V_{\rm th_i i}(\sigma_{\rm io}^{\rm CX} + \sigma_{\rm io}^{\rm elas}) \approx 6 \times 10^3\ {\rm s}^{-1}$ in the

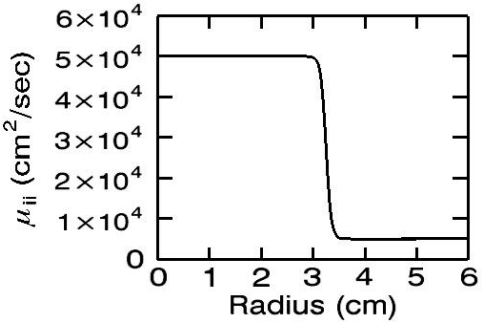

Figure 9. Radial profile of ion–ion collisional viscosity used in turbulent momentum balance.

central plasma region. The ion and neutral temperatures are likely to be peaked at $r = 0$. Since $\mu_{ii} \propto N_i/T_i^{1/2}$ we then surmise that, if the ion temperature profile has a similar shape to the plasma density and electron temperature profiles, the ion viscosity is peaked in the plasma centre and is smaller in the edge region. Exactly what shape the viscosity profile has depends upon the details of the T_i profile. The simplest model for the ion viscosity is a step-like viscous profile that is high in the plasma centre and smaller at the edge of the plasma. The location of the step is constrained by the location of the grad-n_0 region, while the on-axis values are constrained by the central region estimates given above. The ion viscosity in the outer regions is difficult to estimate because there are no reliable ion temperature measurements available from this region. Furthermore, if the neutral gas behaves like an ideal gas, and given the likelihood that the neutral gas temperature is higher in the centre and cooler near the plasma edge, we can then conclude that the neutral gas density is likely depleted in the plasma centre, while near the plasma edge the neutral gas density increases to values that correspond to 3 mTorr at or near room temperature. Thus ν_{i-n} has a minimum in the plasma centre and increases in the outer regions of the plasma. The central chord value of ν_{i-n} would then be approximately equal to the value listed above.

Given these arguments and considerations, we assume a viscosity profile shown in figure 9. We found somewhat surprisingly that the turbulent momentum conservation is insensitive to the details of the ion-neutral flow damping profile, so we simply use a uniform value of $\nu_{i0} = 6 \times 10^3\ s^{-1}$ at all radii since we have no measurements of the neutral spatial profiles. These dissipation profiles are then used in the numerical solution of the turbulent momentum conservation equation given above. Numerically integrating this turbulent momentum balance from $r = 0$ outwards then gives the time-averaged azimuthal ion fluid velocity profile shown as the solid black line in figure 6. This result shows that a shear layer should exist in this plasma, with a peak flow shear located approximately at $r = 3.6$ cm, coincident with a gradient in the viscosity and the gradient in the Reynolds stress. The central ($r < 3$ cm) and outer ($r > 5$ cm) portions of plasma column are then dragged along by viscosity by the outer sheared flow.

5. Turbulent simulations

The fluctuations in this experiment have been shown to be caused by collisional drift turbulence that is sustained by the time-averaged electron pressure gradient and destabilized by electron–ion Coulomb collisions [5]. This class of drift turbulence can be described within the framework of fluid theory and shares the nonlinear dynamics that are thought to be representative of many types of drift turbulence [39,40]. As shown in the literature [34] the dynamics of the turbulence

are described by two coupled dimensionless nonlinear equations describing the evolution of the internal energy ($W_k^n = |n_k|^2$) and the kinetic energy ($W_k^\phi = k_\perp^2 |\phi_k|^2$). The governing equations can then be written in dimensionless form as [34]

$$\frac{\partial n}{\partial t} + \vec{V} \cdot \vec{\nabla}\, n + \frac{V_{\rm de}}{r}\frac{\partial \phi}{\partial \theta} + \omega_{||}(n - \phi) = D\nabla_\perp^2 n, \tag{2a}$$

$$\frac{\partial \nabla_\perp^2 \phi}{\partial t} + (\vec{V} \cdot \vec{\nabla})\nabla_\perp^2 \phi + \omega_{||}\,(n - \phi) = -\nu_{{\rm i}-n}\nabla_\perp^2 \phi + \mu_{\rm ii}\nabla_\perp^4 \phi, \tag{2b}$$

where $\vec{V} = -\vec{\nabla}\,\phi \times \hat{z}$. The spatial scales have been normalized by $\rho_{\rm s} = C_{\rm s}/\Omega_{c_{\rm i}}$, where $C_{\rm s}$ is the ion acoustic speed and $\Omega_{c_{\rm i}}$ is the ion gyrofrequency and the time scales have been normalized by $C_{\rm s}/L_n$, where L_n is the density gradient scale length. The field quantities are 'mixing-length normalized' and are given by $n = (L_n/\rho_{\rm s})\tilde{n}/\langle n\rangle$ and $\phi = (L_n/\rho_{\rm s})e\tilde{\phi}/T_{\rm e}$. In addition, $V_{\rm de}$ is the diamagnetic (electron) velocity, $V_{{\rm th}_{\rm e}}$ is the electron thermal speed and here $\mu_{\rm ii}$ represents the normalized ion viscosity. Note that we explicitly include the term $\nu_{{\rm i}-n}$ to denote the (normalized) linear damping of plasma motion due to ion–neutral collisions [27] (which is neglected in most of the literature). In the limit of small ion Landau damping (which is thought to be true for our experiment) there are three dimensionless parameters which, in the absence of neutral collisions, determine the nonlinear dynamics of collisional drift turbulence: (i) the normalized density gradient scale length $\rho_{\rm S}/L_n$, (ii) the so-called 'adiabatic parameter' $\omega_{||} \equiv k_{||}^2 V_{{\rm th}_{\rm e}}^2/\upsilon_{\rm e}$ (where $\upsilon_{\rm e}$ is the electron collision frequency, so that this parameter quantifies the degree to which the Boltzmann relation $n_{\rm e} = n_0 \exp(-e\phi/k_{\rm B}T_{\rm e})$ is maintained via parallel electron dynamics) and (iii) the normalized ion viscosity $\mu_{\rm ii}$. Drift turbulence occurs typically when $\rho_{\rm S}/L_n \ll 1$ and $\mu_{\rm ii} \ll 1$ (conditions that are marginally satisfied in our experiment, where $\rho_{\rm S}/L_n \sim 0.3$–$0.5$ and $\mu_{\rm ii} \sim 0.2$–0.3 for the conditions shown in figure 1) which then allow the convective derivative term to become important in the fluid momentum equation. In the presence of neutral collisions (which can be important in low-temperature partially ionized laboratory experiments such as ours) the dimensionless ion–neutral momentum exchange collision frequency $\nu_{{\rm i}-n}$ is also relevant, and should be much less than one ($\nu_{{\rm i}-n} \sim 0.01$ in our experiment). Note that this dissipation has the form of a frictional drag, rather than a viscosity, and thus has a form that is identical to flow damping that occurs in toroidal systems due to magnetic pumping and neoclassical viscosity [36]. In the presence of finite parallel electron dissipation ($\omega_{||}L_n/C_{\rm s} \sim 1$ in our experiment), the electrons are no longer able to short circuit a developing potential perturbation by rapidly moving along the magnetic field. As a result the Boltzmann relation $\tilde{n} = n_0 \exp(e\tilde{\phi}/k_{\rm B}T_{\rm e})$ breaks down, density and potential fluctuations become decorrelated and a finite phase shift between these two field quantities occurs, resulting in net transport due to the advection of density perturbations by the associated velocity perturbations.

We have developed a numerical simulation of collisional drift turbulence using this model for comparison with our experimental results. This code solves the Hasegawa–Wakatani collisional drift turbulence model described above in the cylindrical geometry of our experiment and includes ion–neutral flow damping. The code is two-dimensional (i.e. is in r–θ space) and treats the poloidal direction spectrally (using a one-third rule to prevent aliasing) while radial derivatives are found using finite differencing in order to retain the cylindrical geometry of the experiment. The equations are solved by a split implicit/explicit scheme, where the left-hand sides of equations (2*a*) and (2*b*) are first integrated by a second-order Runge–Kutta (leapfrog) scheme (with the nonlinear convolutions calculated in real space), and then the dissipative terms on the right-hand side are solved for implicitly [43]. Finite m fluctuations are all assumed to have a single value of $\omega_{||}$ (equivalent to a single parallel wavenumber),

while the $m = 0$ potential fluctuation is taken to have $k_{||} = 0$ (and so $\omega_{||} = 0$ for these fluctuations). The finite m mode amplitudes go to zero at $r = 0$ and $r = a$ (where a is the radius of the cylinder), while the $m = 0$ potential fluctuation amplitude vanishes at $r = a$ and $\partial\phi_{m=0}/\partial r = 0$ at $r = 0$. To mimic the effects of ionization sources which maintain the equilibrium density profile and prevent quasilinear flattening, the $m = 0$ density fluctuation term is not evolved so that the overall $m = 0$ density component is simply the imposed equilibrium density $\langle n\rangle = n_0 \exp(-0.5r^2/L_n^2)$ (which gives a constant diamagnetic frequency $\omega^* = -m(\rho_s C_s/r)(\mathrm{d}\ln\langle n\rangle/\mathrm{d}r) = m(\rho_s C_s/L_n^2)$). For the work shown here we have used 64 points in the radial direction and 128 azimuthal points (giving 42 meaningful poloidal modes) and in normalized units, $\omega_{||} = 1$, $D = 0.05$, $\nu_{i\text{–}n} = 0.03$, $\mu_{ii} = 0.4$, $\rho_s = 1\,\mathrm{cm}$, $L_n = 2\,\mathrm{cm}$ (corresponding to the parameters used in the momentum balance analysis discussed above, since $C_s = 2 \times 10^5\,\mathrm{cm\,s^{-1}}$ for the conditions of these experiments).

Using this simulation we have begun to numerically explore the nonlinear dynamics of the drift turbulence/zonal flow interactions that are observed in this experiment. First, we have compared the results obtained with this code during the initial linear phase (where unstable modes grow exponentially) with results from a linear eigenmode code [78] which has, in turn, been benchmarked against previously published results [23]. The result shows that the simulation accurately reproduces the initial linear growth phase of the coherent drift wave eigenmodes. Interestingly we find that inclusion of a small amount of radially sheared azimuthal $E \times B$ drift in the linear eigenmodes solution will cause the linear eigenmodes to twist. This effect is similar to that reported by the VINETA group [69], except that in their work the twisting was due to a radial variation in the parallel electron dissipation rate. This twisting is significant because theory indicates that the development of twisted anisotropic fluid eddies is the signature of zonal flow formation from coherent fluid eddies [22, 67]. Thus it appears that any radial variation in either azimuthal $E \times B$ drifts or in the parallel dissipation rate creates the conditions necessary for the onset of zonal flows. Also, once we confirmed the essential linear portions of the code, we benchmarked the nonlinear dynamics of the code by confirming the dual cascade properties (i.e. internal energy to small scales, kinetic energy to large) of the Hasegawa–Wakatani system in two dimensions, as predicted by theory [25, 48] and observed in previous numerical studies [7]. In addition, we have reproduced the results of [3, 35, 49], which showed the formation of large-scale structures and flows with $k_\theta = 0$.

Once these benchmarking activities were completed, we ran simulations of our experiments. The geometry and conditions chosen for this simulation correspond to the conditions in the CSDX device at a magnetic field of 1000 G (i.e. they correspond to the equilibrium conditions shown in figures 1(*a*) and (*b*)). Figure 10 shows snapshots of the fluctuating potential and density distribution during the initial linear growth phase, the development of nonlinear coupling between modes and the formation of a strong zonal flow. The results clearly show the initial development of fluctuations (figures 10(*a*) and (*b*)) consistent with the linear eigenmodes analysis results which we have discussed elsewhere, the subsequent development of a twisting pattern in the mode structure (figures 10(*c*) and (*d*)) and finally the collapse of finite m-number drift fluctuations into an $m = 0$ sheared zonal flow along with a few finite m modes (figures 10(*e*) and (*f*)).

To determine the degree to which these simulation results agree with the experimental results, we have computed the time and flux-surface averaged azimuthal velocity profile from the saturated state shown in figure 11(*f*). The result shown as the red curve in figure 6 shows several similarities to the experimental results. First, the simulation shows that a shear layer should exist in the vicinity of $r \sim 3.6$–4.0 cm. Second, the magnitude of the peak flow velocity, and the radial shearing rate, is fairly close to the experimental result. Third, the central plasma region then spins up due to plasma viscosity. The relative agreement between simulation and

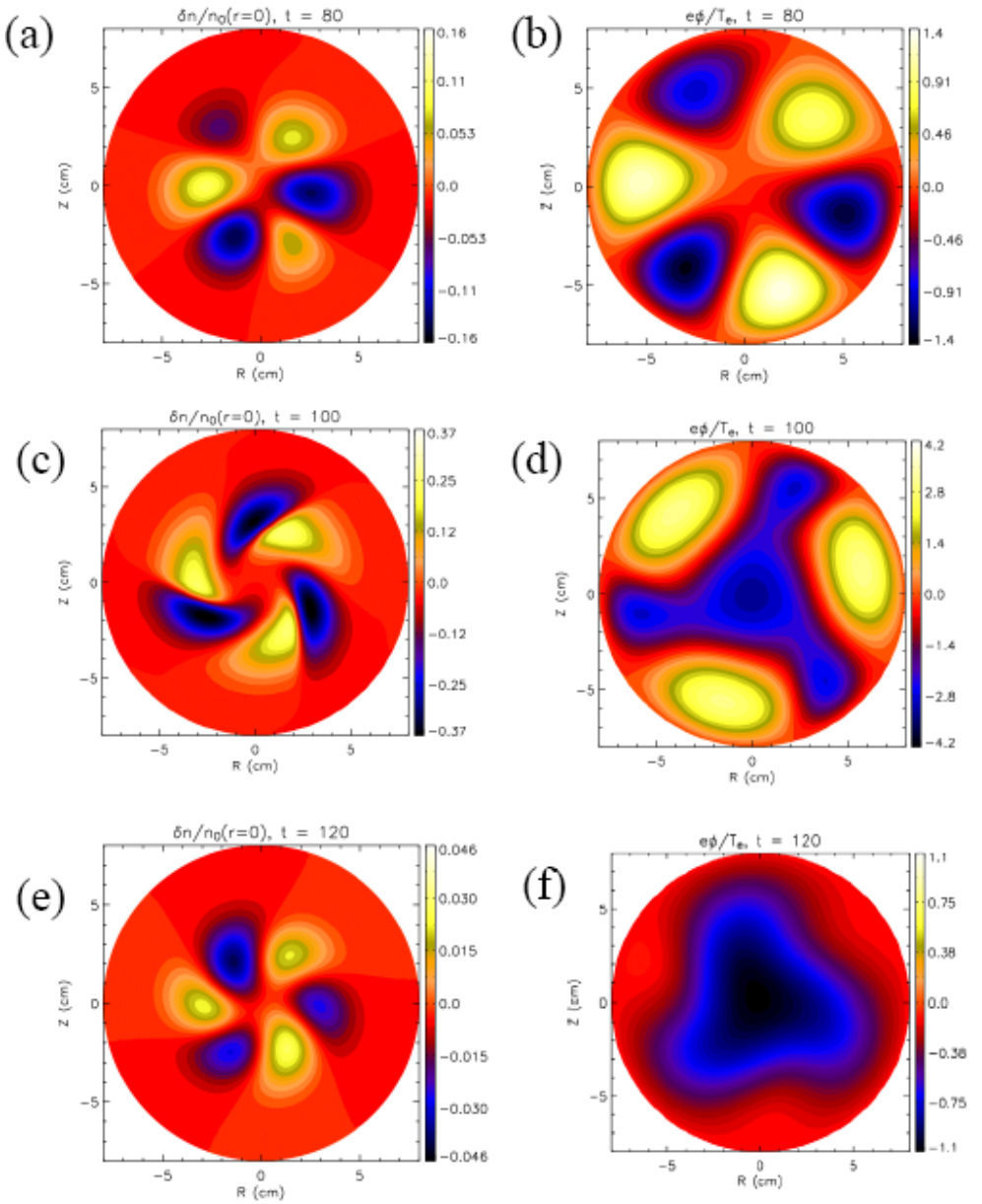

Figure 10. Time-evolution of density fluctuations (panels (*a*), (*c*) and (*e*)) and potential fluctuations (panels (*b*), (*d*) and (*f*)) from a two-field collisional drift turbulence simulation. Panels (*a*) and (*b*) show the early time where the fluctuations resemble the linear eigenmodes solution. Panels (*c*) and (*d*) show the intermediate time where multiple eigenmodes interact nonlinearly, leading to the emergence of a twisted density eigenmode structure. Panels (*e*) and (*f*) show the emergence of a sheared azimuthal flow from the merging of finite m-number vortices.

experiment is particularly surprising given the simplicity and ad hoc assumptions built into the computational model. In addition, we have computed the azimuthal wavenumber spectrum of the potential fluctuations at $r = 3$ cm from the simulation data. The result (figure 11) shows that the potential fluctuation spectrum peaks at $m = 3$ and has significant spectral components

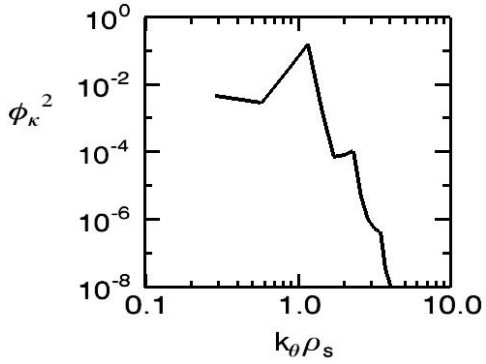

Figure 11. Azimuthal wavenumber spectrum of the saturated state of figures 10(*e*)–(*f*) at $r = 3$ cm. The spectrum peaks at approximately the same location as seen experimentally in figures 4 and 5. The discrete peaks at low wavenumber correspond to low order $m = 1, 2, 3, \ldots$ modes.

for m ranging from $m = 0$ up to $m = 6$–10 or so. This result is reasonably similar to the two-point k-spectra estimates shown in figures 4 and 5. We therefore conclude that this collisional drift turbulence simulation can reproduce the essential features of a turbulent-driven shear flow in a simple configuration.

6. Discussion

As pointed out earlier, a complete demonstration of turbulent-generated shear flow requires several theoretical predictions to be observed in experiment. First, the existence of a shear flow with the correct symmetry properties (e.g. in a cylindrical plasma the shear flow would be azimuthally symmetric) must be demonstrated. Second, the shear flow must be maintained against damping mechanisms by the turbulent Reynolds stress. Third, the resulting shear flow must be of sufficient magnitude that it reduces or eliminates turbulent transport across the shear layer. Finally, this process should be consistent with a relevant theoretical description of the turbulence generation and shear flow maintenance mechanisms. The results presented above are, to our knowledge, the first to satisfy all of these requirements and thus provide a detailed experimental verification of the essential elements of sheared zonal flow generation from drift turbulence in a simple plasma experiment.

Because these results rely critically on the use of Langmuir probes, effects such as non-thermal electron distribution functions can change the relationship between the floating and space potentials and thus cause a systematic error in the measurement of the fluctuating electric field. Such errors would then be carried into the measurements of turbulent transport and thus could potentially impact the conclusions reached in this work. The source for fast electrons would obviously be the plasma source RF antenna region, which is located about 1 m upstream from our probe measurements. The mean free path for electrons that are resonant with the propagating helicon waves (i.e. electrons with energies of tens of electronvolts) in these types of plasmas is of the order of a few tens of centimetres. Thus we would expect that any such particles would likely suffer thermalizing collisions before reaching our probes, minimizing the impact of such effects. We also point out that in a very detailed study [4], the electron distribution function in high density high power helicon plasmas very similar to ours was found to be Maxwellian up to energies $E \sim 10 k_B T_e$ (i.e. up to 25 eV or so), and the fraction of fast ($E > 25$ eV) electrons had to be below the detection limit of 2×10^{-4}. Such a

fraction of fast electrons in our plasma would not produce a large effect on the probe signals. Furthermore, to produce a spurious electric field from the difference in measured V_{float}, any such particles would have to have a different density and/or energy at two probes located 0.5 cm apart. The generation of such particles is thought to occur from a wave–particle resonance in a helicon source, which would generate fast particles in the parallel direction. Helicon waves have a transverse wavelength of the order of the plasma radius, implying that fast particle generation rates would vary only over this spatial scale. Thus it seems unlikely that any such fast particles (whose density is very low as shown by the work of Blackwell *et al*) would then have significantly different distribution functions over such a distance. We conclude that this evidence suggests that fast electrons are probably not a concern here.

In our view, the most serious concern from all probe measurements of fluctuation-induced transport arises from the effect of electron temperature fluctuations. Clearly, if the electron temperature fluctuates then the difference between V_{space} and V_{float} will vary in time, and electron temperature fluctuations will mask themselves as potential (and E-field) fluctuations. We do not know of any reliable T_{e} fluctuation techniques that would allow simultaneous unperturbed V_{float} measurements. The seriousness of this effect on our results depends upon the phase and magnitude of the T_{e} fluctuations relative to the potential fluctuations as has been discussed in many other places (see, e.g. [60]). Recent work [74] suggests that the phase of T_{e} fluctuations relative to space potential fluctuations is such that the gradient in fluctuating floating potential provides a good proxy for the true fluctuating electric field. In the work by Light [53], the electron temperature fluctuations were found to be small in a similar helicon plasma device. If electron temperature fluctuation effects were causing a systematic error in our inferred electric fields and turbulent fluxes, then it would be surprising that the errors worked out to give results that are consistent with turbulent momentum balance and numerical simulation. These observations then weigh against this concern as a serious issue in this work. We note that recently multiple heavy ion beam probe measurements have been used to infer fluxes and zonal flows in confined plasmas [24]. However, lacking such measurements, we provide the results from the V_{float} fluctuations and then point out the assumption of negligible T_{e} fluctuations to the reader. Clearly it would be desirable and useful to investigate this issue further.

7. Conclusions

We have observed the formation of an azimuthally symmetric shear flow in a cylindrical magnetized plasma column that does not have any identifiable external momentum sources. This shear flow is found to be sustained against ion–ion viscosity and against ion–neutral drag via the measured turbulent transport of momentum carried both by the turbulent particle flux and the turbulent Reynolds stress. Because the origins of the turbulence have been identified in this experiment, we infer the existence of a nonlinearly generated transfer of energy from the higher wavenumber turbulent fluctuations into the range of smaller wavenumbers associated with the shear flow. In addition, we can also then justify the use of a two-field fluid-based Hasegawa–Wakatani model for the drift fluctuations. A numerical solution of this model for the conditions of our experiment indicates that such turbulent-driven shear flows spontaneously arise in a simple plasma configuration via the progressive merger of tilted anisotropic vortices that are driven by a collisional drift instability. This phenomena is simply a real-space manifestation of an inverse energy transfer occurring in Fourier space. The magnitude and location of this shear flow is in good agreement with our experimental observations. Taken together, these experimental and computational results support the essential theoretical features expected for zonal flow generation from drift turbulence in magnetized plasmas [20].

There are several issues to explore in the future. First, with appropriate probe array geometries and adequate statistics, the nonlinear energy transfer in a two-field turbulent system can be measured and then compared with the simulations. This effort would address the key underlying nonlinear dynamics of the zonal flow formation and may shed light upon the saturation mechanisms that govern zonal flows. Second, we have not yet made any measurement of the axial wavenumber of the shear flow. Careful alignment of probes would allow this important quantity to be measured and could then allow us to rule out other possible types of azimuthally symmetric oscillations (e.g. ion acoustic waves). Third, fast-framing imaging can be performed of the plasma density fluctuations, and two-dimensional time-delay estimation techniques can be used to infer the turbulent velocity field. If successfully implemented, such algorithms would then allow similar studies to be carried out using imaging diagnostics on tokamak devices. Finally, our recent computational studies of this system indicate that the turbulence and shear flow can exhibit a predator–prey phenomena. Non-stationary data analysis techniques need to be developed and used with our datasets (e.g. wavelet analysis, conditional sampling) in order to examine such dynamics experimentally. In particular, the code suggests that the intensities of the turbulence and zonal flow oscillate with a definite phase relation (as expected from the predator–prey formalism and seen previously by Biskamp and Zeiler [3]), a prediction which one can look for in the experimental data. Recent experimental studies in our device also suggest that the fluctuations become highly intermittent or bursty outside of the shear layer. The present simulations completely fail to capture these potentially important dynamics, and thus additional experimental and computational work is needed on this subject. Finally, it would be interesting to search for similar dynamics in a low-temperature toroidal device in order to avoid end effects and also to examine the effect toroidicity has upon the turbulence, shear flow and coupling between these two types of plasma fluctuations.

Appendix A. derivation of the azimuthal momentum balance equation

In this appendix, we show explicitly the derivation of the azimuthal momentum balance equation used in the text (equation (1)). We begin with the most general form of the ion momentum equation

$$nM\frac{\mathrm{d}\vec{V}_\mathrm{i}}{\mathrm{d}t} = -\vec{\nabla}\, p_\mathrm{i} + \vec{\nabla}\cdot\overleftrightarrow{\pi} + en(\vec{E} + \vec{V}_\mathrm{i}\times\vec{B}) + \vec{R}_\mathrm{i}, \tag{A1}$$

where n is the ion density, p_i is the pressure, $\overleftrightarrow{\pi}$ is the viscosity tensor and $\vec{R}_\mathrm{i}$ the net force on ions due to collisions with other species. For a highly collisional (but not fully ionized) plasma such as the one in CSDX, it can be reduced to

$$nM\frac{\mathrm{d}\vec{V}_i}{\mathrm{d}t} \approx -\vec{\nabla}\, p_i + en(\vec{E} + \vec{V}_\mathrm{i}\times\vec{B}) - nM\upsilon_{\mathrm{i}-n}\,\vec{V}_\mathrm{i} + nM\mu_\mathrm{ii}\nabla_\perp^2\,\vec{V}_\mathrm{i}, \tag{A2}$$

where $\nu_{\mathrm{i}-n}$ is ion–neutral collision rate, the neutrals have been assumed to have negligible velocity and μ_ii is the ion viscosity. If we assume that low ion temperature ($T_\mathrm{i} \leqslant 1$ eV in CSDX, $T_\mathrm{e} \approx 3$ eV) allows us to neglect ion pressure fluctuations, then density can be removed entirely from the equation, and we can write the azimuthal component of equation (A2) as

$$\begin{aligned}&\frac{\partial V_\theta}{\partial t} + V_r\frac{\partial V_\theta}{\partial r} + \frac{V_\theta}{r}\frac{\partial V_\theta}{\partial\theta} + V_z\frac{\partial V_\theta}{\partial z} + \frac{V_r V_\theta}{r} = \\ &\frac{e}{m}(E_\theta - V_r B) - \upsilon_{\mathrm{i}-\mathrm{n}}V_\theta + \mu_\mathrm{ii}\left(\nabla^2 V_\theta + \frac{2}{r^2}\frac{\partial V_r}{\partial\theta} - \frac{V_\theta}{r^2}\right).\end{aligned} \tag{A3}$$

If we now take the time-average of equation (A3), denoting average quantities within brackets, and fluctuating quantities with tildes and further assume that

1. the time-averaged quantities have only a radial spatial dependence and
2. there is no mean radial flow $\langle V_r \rangle$.

Equation (A3) can then be expressed as

$$\left\langle \tilde{V}_r \frac{\partial \tilde{V}_\theta}{\partial r} + \frac{\tilde{V}_\theta}{r}\frac{\partial \tilde{V}_\theta}{\partial \theta} + \tilde{V}_z \frac{\partial \tilde{V}_\theta}{\partial z} + \frac{\tilde{V}_r \tilde{V}_\theta}{r} \right\rangle = -\upsilon_{i\text{–}n}\langle V_\theta \rangle + \mu_{ii}\left(\frac{\partial^2 \langle V_\theta \rangle}{\partial r^2} + \frac{1}{r}\frac{\partial \langle V_\theta \rangle}{\partial r} - \frac{\langle V_\theta \rangle}{r^2} \right). \tag{A4}$$

The final assumption is that the fluctuating velocities are $\vec{E} \times \vec{B}$ dominated (i.e. ignoring corrections due to polarization/inertia and dissipative terms) and therefore incompressible since $\vec{B} = B\hat{z}$ in CSDX, so we can then make use of the following relation:

$$\tilde{V}_\theta(\vec{\nabla} \cdot \tilde{\vec{V}}) = \tilde{V}_\theta \left(\frac{\partial \tilde{V}_r}{\partial r} + \frac{\tilde{V}_r}{r} + \frac{1}{r}\frac{\partial \tilde{V}_\theta}{\partial \theta} + \frac{\partial \tilde{V}_z}{\partial z} \right) = 0. \tag{A5}$$

Adding the time average of equation (A5) to the left-hand side (LHS) of equation (A4), we find

$$\begin{aligned} \text{LHS} &= \left\langle \tilde{V}_\theta \left(\frac{\partial \tilde{V}_r}{\partial r} + \frac{\tilde{V}_r}{r} + \frac{1}{r}\frac{\partial \tilde{V}_\theta}{\partial \theta} + \frac{\partial \tilde{V}_z}{\partial z} \right) + \tilde{V}_r \frac{\partial \tilde{V}_\theta}{\partial r} + \frac{\tilde{V}_\theta}{r}\frac{\partial \tilde{V}_\theta}{\partial \theta} + \tilde{V}_z \frac{\partial \tilde{V}_\theta}{\partial z} + \frac{\tilde{V}_r \tilde{V}_\theta}{r} \right\rangle \\ &= \left\langle \tilde{V}_r \frac{\partial \tilde{V}_\theta}{\partial r} + \tilde{V}_\theta \frac{\partial \tilde{V}_r}{\partial r} + \frac{2\tilde{V}_r \tilde{V}_\theta}{r} + \frac{2\tilde{V}_\theta}{r}\frac{\partial \tilde{V}_\theta}{\partial \theta} + \tilde{V}_z \frac{\partial \tilde{V}_\theta}{\partial z} + \tilde{V}_\theta \frac{\partial \tilde{V}_z}{\partial z} \right\rangle \\ &= \frac{1}{r^2}\frac{\partial}{\partial r}(r^2 \langle \tilde{V}_r \tilde{V}_\theta \rangle) + \frac{1}{r}\frac{\partial \langle \tilde{V}_\theta^2 \rangle}{\partial \theta} + \frac{\partial \langle \tilde{V}_\theta \tilde{V}_z \rangle}{\partial z} \\ &= \frac{1}{r^2}\frac{\partial}{\partial r}(r^2 \langle \tilde{V}_r \tilde{V}_\theta \rangle), \end{aligned} \tag{A6}$$

where we have made explicit use of our assumption that all time-averaged quantities have no azimuthal or axial gradients. Therefore, the time averaged version of the ion azimuthal momentum equation is given by

$$\frac{1}{r^2}\frac{\partial}{\partial r}(r^2 \langle \tilde{V}_r \tilde{V}_\theta \rangle) = -\upsilon_{i\text{–}n}\langle V_\theta \rangle + \mu_{ii}\left(\frac{\partial^2 \langle V_\theta \rangle}{\partial r^2} + \frac{1}{r}\frac{\partial \langle V_\theta \rangle}{\partial r} - \frac{\langle V_\theta \rangle}{r^2} \right). \tag{A7}$$

Acknowledgments

The authors wish to thank P H Diamond, S-I Itoh, K Itoh and F Spineanu for many valuable suggestions and conversations. Discussions with S I Itoh, K Itoh and F Spineanu were made possible by the Grant-in-Aid for Specially-Promoted Research of MEXT, Japan (16002005). This research was performed under grants DE-FG02-04ER54773 and DE-FG02-04ER54734. C H performed this research under appointment to the Fusion Energy Postdoctoral Research Program administered by the Oak Ridge Institute for Science and Education under contract number DE-AC05-00OR22750 between the US Department of Energy and Oak Ridge Associated Universities.

References

[1] Beall J M, Kim Y C and Powers E J 1982 Estimation of wavenumber and frequency spectra using fixed probe pairs *J. Appl. Phys.* **53** 3933

[2] Beyer P, Benkadda S, Garbet X and Diamond PH 2000 Nondiffusive transport in tokamaks: three-dimensional structure of bursts and the role of zonal flows *Phys. Rev. Lett.* **85** 4892

[3] Biskamp D and Zeiler A 1995 Nonlinear instability mechanism in 3D collisional drift-wave turbulence *Phys. Rev. Lett.* **74** 706

[4] Blackwell D *et al* 2001 *Plasma Sources. Sci. Technol.* **10** 226

[5] Burin M, Antar G, Crocker N and Tynan G 2005 On the transition to drift turbulence in a magnetized plasma column *Phys. Plasmas* **12** 052320

[6] Busse F H 1994 Convection driven zonal flows and vortices in the major planets *Chaos* **4** 123

[7] Carmargo S J, Biskamp D and Scott B D 1995 Resistive Drift-wave Turbulence *Phys. Plasmas* **2** 48

[8] Chen F F 1964 Normal modes of an electrostatic ion wave in an inhomogenous *Plasma Phys. Fluids* **7** 949

[9] Chen F F 1965a Effect of sheaths on drift instabilities in thermionic plasmas *Phys. Fluids* **8** 752

[10] Chen F F 1965b Resistive overstability and anomalous diffusion *Phys. Fluids* **8** 912

[11] Chen F F 1965c University overstability of a resistive inhomogenous plasma *Phys. Fluids* **8** 1323

[12] Chen F F 1966 Microinstability and shear stabilization of a low β rotating resistive plasma *Phys. Fluids* **9** 965

[13] Chen L, Lin Z, White R B and Zonca F 2001 Nonlinear zonal dynamics of drift and drift-Alfven turbulence in tokamak plasmas *Nucl. Fusion* **41** 747

[14] Chiu J S and Sen A K 1999 Experimental determination of a nonlinear dynamic model of plasma turbulence using feedback control *Phys. Rev. Lett.* **83** 5503

[15] Chu T K, Coppi B, Hendel H W and Perkins F W 1969 Drift instabilities in a uniformly rotating plasma cylinder *Phys. Fluids* **12** 203

[16] Chu T K, Hendell H W and Simonen T C 1973 Parametric effects as the mechanism for energy spreading in wave number space of the drift instability *Phys. Fluids* **16** 2034

[17] Coda S, Porkolab M and Burrell K H 2001 *Phys. Rev. Lett.* **86** 4835

[18] Conway G D *et al* 2005 Direct measurement of zonal flows and geodesic acoustic mode oscillations in ASDEX Upgrade using Doppler reflectometry *Plasma Phys. Control. Fusion* **47** 1165

[19] Diamond P H, Rosenbluth M N, Hinton F, Malkov M, Fleischer J and Smolyakov A 2000 Dynamics of zonal flows and self-regulating drift-wave turbulence *Proc. of the 17th IAEA Fusion Energy Conf. (Yokohama, Japan, 19–24 October 1998)* IAEA-CN-69/TH3/1

[20] Diamond P H, Itoh S I, Itoh K and Hahm T S 2005 Zonal flows in plasma—a review *Plasma Phys. Control. Fusion* **47** R35–161

[21] Drake J F, Guzdar P N and Hassam A B 1988 Streamer formation in plasma with a temperature gradient *Phys. Rev. Lett.* **61** 2205

[22] Drake J F *et al* 1992 Peeling of convection cells and the generation of sheared flow *Phys. Fluids-B Plasma Phys.* **4** 488

[23] Ellis R F, Marden-Marshall E and Majeski R 1980 Collisional drift instability of a weakly ionized argon plasma *Plasma Phys.* **22** 113

[24] Fujisawa A *et al* 2004 Identification of zonal flows in a toroidal plasma *Phys. Rev. Lett.* **93** 165002–1

[25] Gang F Y, Diamond P H, Crotinger J A and Koniges A E 1991 Statistical dynamics of dissipative drift wave turbulence *Phys. Fluids B-Plasma Phys.* **3** 955

[26] George J Experimental study of linear resistive drift waves in a cylindrical helicon plasma device *M S Thesis* Department of Mechanical and Aerospace Engineering, UCSD

[27] Gondarenko N A and Guzdar P N 1999 Gradient drift instability in high latitude plasma patches: ion inertial effects *Geophys. Res. Lett.* **26** 3345

[28] Hai F and Wong A Y 1970 Parametric mode-mode coupling between drift waves in plasmas *Phys. Fluids* **13** 672

[29] Hardin R, Sun X and Scime E E 2004 *Rev. Sci. Instrum.* **75** 4103

[30] Harrison G R 1949 *J. Opt. Soc. Am.* **39** 522

[31] Harrison G R *et al* 1952 *J. Opt. Soc. Am.* **42** 706

[32] Hasegawa A and Mima K 1978 Pseudo-three-dimensional turbulence in magnetized nonuniform plasma *Phys. Fluids* **21** 87

[33] Hasegawa A, Maclennan C G and Kodama Y 1979 Nonlinear behavior and turbulence spectra of drift waves and Rossby waves *Phys. Fluids* **22** 2122

[34] Hasegawa A and Wakatani M 1983 Plasma edge turbulence *Phys. Rev. Lett.* **50** 682

[35] Hasegawa A and Wakatani M 1987 Self-organization of electrostatic turbulence in a cylindrical plasma *Phys. Rev. Lett.* **59** 1581
[36] Hassam A B and Drake J F 1993 Spontaneous poloidal spin-up of tokamak plasmas: Reduced equations, physical mechanism, and sonic regimes *Phys. Fluids* B **5** 4022
[37] Hendel H W, Chu T K and Simonen T C 1969 *Phys. Fluids* **11** 2426
[38] Holland C *et al* 2004 Investigation of the time-delay estimation methode for turbulent velocity inference *Rev. Sci. Instrum.* **75** 4278–80 Part 2
[39] Horton W 1984 Drift turbulence *Handbook of Plasma Physics* vol 2 *Basic Plasma Physics* ed M N Rosenbluth and R Z Sagdeev (Amsterdam: Elsevier)
[40] Horton W 1999 Drift waves and transport *Rev. Mod. Phys.* **71** 735
[41] Hutchinson I H 2002 *Plasma. Phys. Control. Fusion* **44** 953
[42] Jakubowski M, Fonck R J and McKee G R 2002 *Phys. Rev. Lett.* **89** 265003
[43] Karniadakis G E, Israeli M and Orszag S A 1991 High-order splitting methods for the incompressible navier-stokes equations *J. Comp. Phys.* **97** 414
[44] Kim J S, Durst R D, Fonck R J, Fernandez E, Ware Aand Terry P W 1996 Technique for the experimental estimation of nonlinear energy transfer in fully developed turbulence *Phys. Plasmas* **3** 3998
[45] Kim J S, Fonck R J, Durst R D, Fernandez E, Terry P W, Paul S F and Zarnstorff M C 1997 Measurement of nonlinear energy transfer in turbulence in the tokamak fusion test reactor *Phys. Rev. Lett.* **79** 841
[46] Kim Y C and Powers E J 1979 Digital bispectral analysis and its applications to nonlinear wave interactions *IEEE Trans. Plasma Sci.* **2** 120
[47] Klinger T, Latten A, Piel A, Bonhomme G and Pierre T 1997 Chaos and turbulence studies in low- beta plasmas *Plasma Phys. Control. Fusion* **39** B145
[48] Koniges A E, Crotinger J A, Dannevik W P, Carnevale G F, Diamond P H and Gang F Y 1991 Equilibrium spectra and implications for a two-field turbulence model *Phys. Fluids B-Plasma Phys.* **3** 1297
[49] Korsholm S B, Michelsen P K and Naulin V 1999 Resistive drift wave turbulence in a three-dimensional geometry *Phys. Plasmas* **6** 2401
[50] Korsholm S B, Michelsen P K, Naulin V, Rasmussen J J, Garcia L, Carreras B A and Lynch V E 2001 Reynolds stress and shear flow generation *Plasma Phys. Control. Fusion* **43** 1377
[51] Kraichnan T H 1967 Inertial range transfer in two-dimensional turbulence *Phys. Fluids* **10** 1417
[52] Liewer P 1985 Measurements of microturbulence in tokamaks and comparisons with theories of turbulence and anomalous transport *Nucl. Fusion* **25** 543
[53] Light M 2000 *PhD Dissertation* Department of Electrical Engineering, UCLA
[54] Light M, Chen F F and Colestock P L 2001 *Phys. Plasmas* **8** 4675
[55] McDaniel E W, Mitchell J B A and Rudd M E 1993 *Atomic Collisions: Heavy Particle Projectiles* (New York: Wiley)
[56] McIntyre M E 1989 On the Antarctic ozone hole *J. Atmos. Terr. Phys.* **51** 29
[57] McKee G R *et al* 2003 *Phys. Plasmas* **10** 1712
[58] McWilliams J C 1984 The emergence of isolated coherent vortices in turbulent flow *J. Fluid Mech.* **146** 21
[59] Mizuta R and Yoden S 2001 Chaotic mixing and transport barriers in an idealized stratospheric polar vortex *J. Atmos. Sci.* **58** 2616
[60] Moyer R A *et al* 1995 *Phys. Plasmas* **2** 2397
[61] Moyer R A, Tynan G R, Holland C and Burin M J 2001 Increased nonlinear coupling between turbulence and low-frequency fluctuations at the L-H transition *Phys. Rev. Lett.* **87** 135001/1-4
[62] Nevins W 2002 private communication
[63] Paret J and Tabeling P 1997 Experimental observation of the two-dimensional inverse energy cascade *Phys. Rev. Lett.* **79** 4162–5
[64] Politzer P 1971 Drift instability in collisionless alkali metal plasmas *Phys. Fluids* **11** 2410
[65] Pope E 2002 *Turbulent Flow* (Cambridge: Cambridge University Press)
[66] Rosenbluth M N and Hinton F L 1998 Poloidal flow driven by ion-temperature-gradient turbulence in tokamaks *Phys. Rev. Lett.* **80** 724
[67] Rosenbluth M N and Shapiro V D 1994 Analytical model of the tilting instability *Phys. Plasmas* **1** 222
[68] Sagdeev R Z and Galeev A A 1969 *Nonlinear Plasma Phys.*
[69] Schroder C, Grulke O, Klinger T and Naulin V 2004 Spatial mode structure of electrostatic drift waves in a collisional cylindrical helicon plasma *Phys. Plasmas* **11** 4249
[70] Shats M G and Solomon W M 2002 Experimental evidence of self-regulation of fluctuations by time-varying flows *Phys. Rev. Lett.* **88** 045001–1
[71] Shats M G and Solomon W M 2002 Zonal flow generation in the improved confinement mode plasma its role in confinement bifurcations *New J. Phys.* 4 30.1–30.14

[72] Shats M G, Xia H and Punzmann H 2005 Spectral condensation of turbulence in plasmas and fluids and its role in the transitions in toroidal plasmas *Phys. Rev. E* **71** 046409
[73] Shikama T, Kado S, Okamoto A Kajita S and Tanaka S 2005 *Phys. of Plasma.* **12** 044504
[74] Stroth U 2005 private communication
[75] Tabeling P 2002 Two-dimensional turbulence: A physicist's approach *Phys. Rep.* **362** 1
[76] Tynan G R *et al* 1997 Characterization of an azimuthally symmetric helicon wave high density plasma source *J. Vac. Sci. Technol.* A **15** 2885
[77] Tynan G R, Moyer R A, Burin M J and Holland C 2001 On the nonlinear dynamics of shear-flow decorrelation and zonal flow generation *Phys. Plasmas* **8** 2691
[78] Tynan G R *et al* 2004 Radially sheared azimuthal flows and turbulent transport in a cylindrical plasma device *Phys. Plasmas* **11** 5195
[79] Wong A Y, Cheung P Y and Tanikawa T 1984 Evolution from coherence to turbulence in plasmas *Statistical Physics and Chaos in Fusion Plasmas* ed Horton and Reichl (New York: Wiley) p 131
[80] Xia H and Shats M G 2003 Inverse energy cascade correlated with turbulent structure generation *Phys. Rev. Lett.* **91** 155001–1
[81] Xia H and Shats M G 2004 Spectral energy transfer and generation of turbulent structures in toroidal plasma *Phys. Plasmas* 11 561
[82] Xu Y H *et al* 2000 Role of reynolds stress-induced poloidal flow in triggering the transition to improved ohmic confinement in the HT-6M tokamak *Phys. Rev. Lett.* **84** 3867